

# Non-Newtonian stagnant lid convection and the thermal evolution of Ganymede and Callisto

J. Freeman\*

*School of Mathematical Sciences, Monash University, Clayton Victoria 3800, Australia*

Received 2 March 2004; received in revised form 20 July 2005; accepted 5 October 2005

Available online 13 December 2005

## Abstract

The thermal evolution of Ganymede and Callisto was calculated using a realistic water ice heat flux scaling law. This scaling was derived from numerical studies of thermal convection with a stress and temperature dependent viscosity relationship that is descriptive of dislocation creep of crystalline water ice I. This result is then compared with that determined using a non-Newtonian silicate like rheology, a strongly temperature dependent Newtonian rheology and an isoviscous scaling law. In all cases, the stagnant lid convection models resulted in warmer internal mantle temperatures and thicker conductive lids than the isoviscous scaling law, in agreement with theory. It was found that the isoviscous thermal evolution models for each icy satellite gave cool, frozen models, whilst the stagnant lid scaling laws resulted in warmer satellite interiors. High viscosity models resulted in extensive melting of the icy mantle. The presence of subsurface oceans within the icy Galilean satellites has been inferred from the Galileo data and stagnant lid thermal convection is one mechanism through which a subsurface ocean may form.

© 2005 Elsevier Ltd. All rights reserved.

*Keywords:* Thermal evolution; Icy satellite; Mantle convection

## 1. Introduction

The Galileo spacecraft provided a detailed set of data describing the surface features, internal structure and magnetic fields of the icy Galilean satellites Europa, Ganymede and Callisto. Comparative studies of the surfaces of the icy Galilean satellites indicate that Europa has a young sparsely cratered surface whilst the surfaces of both Ganymede and Callisto are considerably older.

Ganymede is the largest satellite in the solar system and displays a complex surface morphology (McKinnon and Parmentier, 1986; Kirk and Stevenson, 1987; Mueller and McKinnon, 1988; Showman et al., 1997; Dombard and McKinnon, 2000, 2001; Schenk et al., 2001). Ganymede's mean density of  $1.936 \text{ g cm}^{-3}$  indicates nearly equal masses of rock and ice. Data from two Galileo flybys gave Ganymede's axial moment of inertia to be  $0.3105 \pm 0.0028$  (Anderson et al., 1996). This suggests differentiation between silicates and ices within the satellite. Interior

models suggest that Ganymede is differentiated (Kirk and Stevenson, 1987; McKinnon and Parmentier, 1986; Mueller and McKinnon, 1988; Anderson et al., 1996; Schubert et al., 1996; Crary and Bagenal, 1998) into an outermost  $\sim 800 \text{ km}$  thick ice layer and an underlying silicate mantle of a density of  $3\text{--}4 \text{ g cm}^{-3}$  (Anderson et al., 1996). Structural modeling indicates that a central iron sulfide core with a radius up to 50% of Ganymede's radius is allowed, and the existence of Ganymede's magnetic field is suggestive of such a core (Schubert et al., 1996; Kivelson et al., 1996; Gurnett et al., 1996; Crary and Bagenal, 1998).

Callisto's surface morphology is characterized by a heavily cratered terrain (Greeley et al., 2000). Numerous impact remnants scar the surface of the satellite and crater count studies indicate that the satellite's surface is old (Zhanle et al., 1998). Results from the Galileo science mission shows that Callisto is devoid of any long-term endogenic processes and the surface displays no evidence of cryovolcanic flows, as observed on Ganymede (Schenk et al., 2001). With a mean density of  $1.85 \text{ g cm}^{-3}$ , Callisto consists of nearly equal fractions of ice and silicate materials. Structural models describing the interior of

\*Tel.: +61 2 6125 8365.

E-mail address: [justin.freeman@anu.edu.au](mailto:justin.freeman@anu.edu.au).

Callisto have included both fully differentiated (silicate interior overlain by ice mantle), homogeneous (uniform ice–silicate mixtures) and partially differentiated (silicate–ice cores with icy mantles) scenarios (Schubert et al., 1981; Anderson et al., 1997, 1998a; McKinnon and Parmentier, 1986; Mueller and McKinnon, 1988; McKinnon, 1997).

The normalized axial moment of inertia for Callisto (assuming hydrostatic equilibrium) was determined to be  $C/MR^2 = 0.359 \pm 0.005$  (Anderson et al., 1998a). This value is less than that expected for a homogeneous body of Callisto’s mass and radius, implying a partially differentiated internal structure. Magnetic field data from three Galileo flybys of Callisto indicate the distinct signature of an induced magnetic field (Gurnett et al., 1997; Khurana et al., 1997; Kivelson et al., 1999; Zimmer et al., 2000). The origin of the weak magnetic field has been hypothesized to be due to the interaction of the ambient background Jovian field with an electrolytic conducting liquid layer beneath the crust of Callisto (Kivelson et al., 1999; Zimmer et al., 2000).

### 1.1. Rheology

Materials, such as silicates and water ice, have strongly temperature and stress dependent rheologies, suggesting that stagnant lid convection is the appropriate convective style for planets. These are non-Newtonian fluids in which the strain rate is proportional to the stress raised to a power,  $n$ . For silicate materials, the value of  $n$  is 3 (Karato and Wu, 1993), whilst dislocation creep of water ice I is described by a stress dependence of  $n \sim 4$  (Durham et al., 1992; Goldsby and Kohlstedt, 2001). Solomatov and Moresi (1997), using a silicate like rheology demonstrated the existence of the three convective regimes for the non-Newtonian viscosity convection. These convective regimes were also confirmed to exist (at a larger temperature determined viscosity contrast than the  $n = 3$  rheology) for

a non-Newtonian water ice rheology (Freeman et al., 2004).

In this study, I model the thermal evolution of Ganymede and Callisto using the heat flux scaling relationships derived from studies of isoviscous, strongly temperature dependent viscosity stagnant lid and non-Newtonian viscosity convection.

### 1.2. Thermal evolution

A heat flux scaling law relates the vigor of convection, the Rayleigh number  $Ra$ , to the efficiency of convective heat transport, the Nusselt number  $Nu$ , via a simple relationship,

$$Nu = aRa^b, \quad (1)$$

where  $a$  and  $b$  are constants. Thermal convection with a variable (i.e. temperature and/or stress dependent) viscosity have shown that the scaling law is different from that of the constant viscosity case. Laboratory and numerical simulation of isoviscous thermal convection have shown that this system is characterized by symmetrical thermal boundary layer thicknesses and uniform internal temperatures (Nataf and Richter, 1982; Richter et al., 1983; Morris and Canright, 1984; Ogawa et al., 1991; Fowler, 1985; Davaille and Jaupart, 1993; Solomatov, 1995) (see Fig. 1). With a temperature and/or stress dependent viscosity, thermal convection may operate in one of the three regimes. These regimes are the small viscosity contrast regime, the transitional regime and the stagnant lid regime.

## 2. Model

Many studies of the thermal evolution of the inner planets of the solar system have employed a parameterized approach (Schubert et al., 1979; Spohn and Schubert, 1982; Stevenson et al., 1983; Honda, 1995; Honda and Iwase, 1996; McNamara and van Keken, 2000). Direct application of the method to modeling the thermal evolution

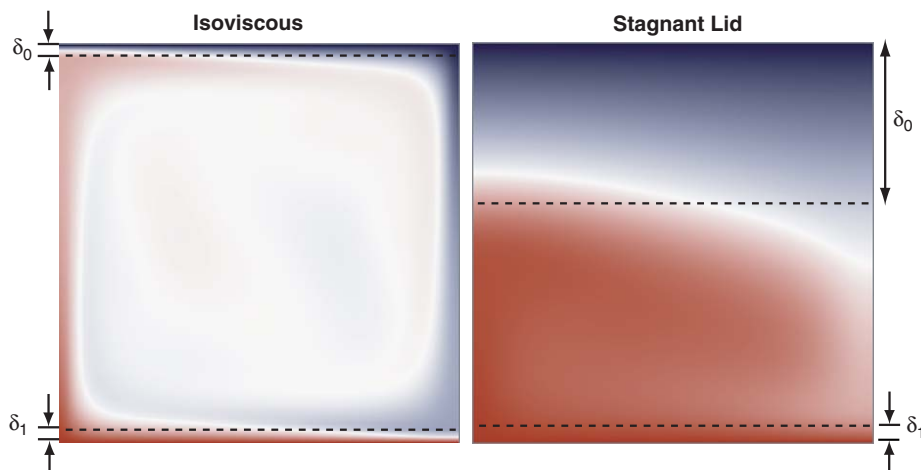


Fig. 1. Boundary layer thickness for both isoviscous and stagnant lid convection. Shown in the figure is the temperature field and  $Ra = 10^6$  for both models. The viscosity contrast for the stagnant lid temperature dependent viscosity model is  $\Delta\eta = 10^9$ .

of an icy satellite have also been previously undertaken (Ellsworth and Schubert, 1983; Deschamps and Sotin, 2001; Hussmann et al., 2002). An energy conservation equation is solved for each layer,

$$v\rho c_p \frac{dT_c}{dt} = q_{in}a_{bot} - q_{out}a_{top} + Qv, \quad (2)$$

where  $v$  is the volume of the layer,  $\rho$  is the density,  $c_p$  is the specific heat,  $T_c$  is the average temperature,  $Q$  is the volumetric heat production and  $a_{bot}$  and  $a_{top}$  are the areas of the bottom and top boundaries respectively.  $q_{in}$  and  $q_{out}$  are the heat flows into and out of the layer, respectively. These are given by the heat flow relationship,

$$q = \frac{k\Delta T_\delta}{d} \left( \frac{Ra}{Ra_c} \right)^b, \quad (3)$$

where  $k$  is the thermal conductivity,  $\Delta T_\delta$  is the temperature drop over the boundary layer,  $d$  is the thickness of the convecting layer, the exponent  $b$  is a constant,  $Ra_c$  is the critical Rayleigh number and  $Ra$  is the Rayleigh number,

$$Ra = \frac{\alpha g \rho \Delta T d^3}{\kappa \eta(T)}, \quad (4)$$

where  $\alpha$  is the thermal expansivity,  $g$  is acceleration due to gravity,  $\rho$  is density,  $\Delta T$  is the temperature drop across the convecting layer,  $\kappa$  is the thermal diffusivity and  $\eta(T)$  is the viscosity at the average temperature given by,

$$\eta(T_i) = \eta_0 \exp \left[ l \left( \frac{T_m}{T} - 1 \right) \right], \quad (5)$$

where  $\eta_0$  is the viscosity of the material at the zero pressure melting point,  $T_m$  is the material melting temperature,  $T$  is the average temperature and  $l = E/(RT_m)$  is a constant ( $R$  is the gas constant). The boundary layer thickness is given by

$$\delta = d \left( \frac{Ra_c}{Ra} \right)^b. \quad (6)$$

The heat production is represented as the sum of heat produced for each of the radioactive species  $^{235}\text{U}$ ,  $^{238}\text{U}$ ,  $^{232}\text{Th}$  and  $^{40}\text{K}$ . The heat production rate due to the decay of radioactive nuclides is given by

$$Q(t) = \sum_{i=1}^n Q_i A_i \exp(-\lambda_i t), \quad (7)$$

where  $Q_i$  is the heat production rate of species  $i$  at time  $t = 0$ ,  $A_i$  is the initial abundance of species  $i$  and  $\lambda_i$  is the decay constant of species  $i$ . The volumetric abundance of the radioactive species,  $^{40}\text{K}$ ,  $^{232}\text{Th}$ ,  $^{235}\text{U}$  and  $^{238}\text{U}$ , is taken from Turcotte and Schubert (1982).

For the subsequent layered models (ranging from two-layer models up to five-layer models with distinct rheologies) the lower thermal boundary layer is removed. An example of this is shown in Fig. 2. The lower thermal boundary layer is small when considering strongly temperature dependent viscosity convection. This method of

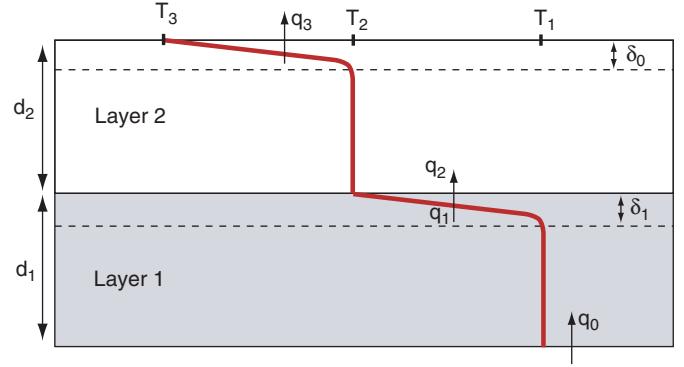


Fig. 2. Two-layer thermal evolution problem description.

treating the lower boundary layer follows the method of Honda (1995) and Honda and Iwase (1996).

For a multi-layered model with  $n$  layers, the following relationships are given for the heat flux:

$$q_{n,in} = q_{n-1,out}, \quad (8)$$

$$q_{n,out} = \frac{k(T_n - T_{n+1})}{d_n} \left( \frac{Ra_n}{Ra_c} \right)^b \quad (9)$$

and the Rayleigh number for layer  $n$  is,

$$Ra_n = \frac{\alpha_n \rho_n g (T_n - T_{n+1}) d_n^3}{\kappa_n \eta(T_n)}. \quad (10)$$

A satellite model with  $m$  layers gives a system of  $m$  coupled ordinary differential equations which may be solved numerically with a given initial temperature,  $T_{0,n}$  for each layer and a given surface temperature,  $T_s$ . The heat flux into the deepest layer, layer  $m$ , is zero, and continuity of heat flux between layers allows for the integration of Eq. (2) for each layer.

### 3. Thermal evolution of the icy Jovian satellites

The simple structural models of Prentice (2001) were employed as initial conditions for the thermal evolution models. For each model, an initial temperature in each layer is assumed. This choice is somewhat arbitrary and has been shown to have no drastic effect on the long-term thermal evolution of the satellite (Ellsworth and Schubert, 1983) (see Fig. 4). Parameters for the satellite models are given in Table 1 and Fig. 3.

Heat transfer through the satellite interior is parameterized with four different models describing the Nusselt number–Rayleigh number relationship. I compare the time evolution of the temperature of the satellite interior and the surface heat flux with the following heat flux scaling laws: isoviscous scaling law (Hansen and Yuen, 1993)

$$Nu = 0.250 Ra^{0.323}, \quad (11)$$

a variable viscosity Newtonian stagnant lid scaling law (Moresi and Solomatov, 1995)

$$Nu = 1.89\theta^{-1.02} Ra^{0.2}, \quad (12)$$

a non-Newtonian silicate like rheology with a stress dependence of  $n = 3$  given by (Solomatov and Moresi, 2000)

$$Nu = 2.1\theta^{-1.333} Ra_i^{0.333}, \quad (13)$$

and a non-Newtonian water ice like rheology with a stress dependence of  $n = 4$  (Freeman et al., 2004)

$$Nu = 0.96\theta^{-1.6} Ra_i^{0.66}. \quad (14)$$

In Eqs. (12)–(14),  $\theta$  is calculated according to

$$\theta = \ln(\Delta\eta), \quad (15)$$

where  $\Delta\eta = (\eta_{\text{surface}} - \eta_{\text{base}})$ .

Table 1  
Parameters used in the thermal evolution models.

| Parameter                      | Value  | Units                             | Ref. |
|--------------------------------|--|-----------------------------------|------|
| $\alpha_{\text{ice}}$          | $2.5 \times 10^{-7} T - 1.25 \times 10^{-5}$ | $\text{K}^{-1}$                   | A    |
| $c_{\text{ice}}$               | $7.037T + 185.0$                             | $\text{J kg}^{-1} \text{K}^{-1}$  | A    |
| $k_{\text{ice}}$               | $4.8812 \times 10^2 / T + 0.4685$            | $\text{W m}^{-1} \text{K}^{-1}$   | A    |
| $T_{m,\text{ice}}$             | 277  | K                                 |      |
| $\alpha_{\text{sil}}$          | $3 \times 10^{-5}$                           | $\text{K}^{-1}$                   | A    |
| $c_{\text{sil}}$               | 1250   | $\text{J kg}^{-1} \text{K}^{-1}$  | A    |
| $k_{\text{sil}}$               | 5.6  | $\text{W m}^{-1} \text{K}^{-1}$   | A    |
| $E_{\text{sil}}$               | 525  | $\text{kJ mol}^{-1}$              | B    |
| $T_{m,\text{sil}}$             | 1000   | K                                 |      |
| $T_s$                          | 103.0  | K                                 |      |
| $R$                            | 8.3144                                       | $\text{J mol}^{-1} \text{K}^{-1}$ |      |
| $\rho_{\text{ice I}}$          | 950  | $\text{kg m}^{-3}$                |      |
| $E_{\text{ice I}}$             | 60.0   | $\text{kJ mol}^{-1}$              |      |
| $\rho_{\text{ice II}}$         | 1170   | $\text{kg m}^{-3}$                |      |
| $E_{\text{ice II}}$            | 55.0   | $\text{kJ mol}^{-1}$              |      |
| $\rho_{\text{ice VI}}$         | 1310   | $\text{kg m}^{-3}$                |      |
| $E_{\text{ice VI}}$            | 136.0  | $\text{kJ mol}^{-1}$              |      |
| $\rho_{\text{ice VIII}}$       | 1500   | $\text{kg m}^{-3}$                |      |
| $E_{\text{ice VIII}}$          | 66.0   | $\text{kJ mol}^{-1}$              |      |
| $\rho_{\text{hydrated sil}}$   | 2500   | $\text{kg m}^{-3}$                |      |
| $\rho_{\text{dehydrated sil}}$ | 3500   | $\text{kg m}^{-3}$                |      |
| $g_{\text{Ganymede}}$          | 1.37   | $\text{m s}^{-2}$                 |      |
| $g_{\text{Callisto}}$          | 1.24   | $\text{m s}^{-2}$                 |      |

References; A: Ellsworth and Schubert (1983), B: Karato and Wu (1993). Water ice data from Durham and Stern (2001).

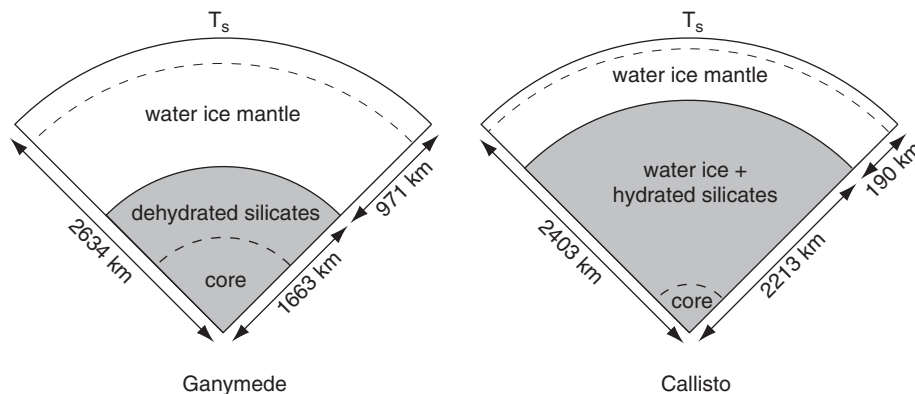


Fig. 3. Internal structure models for the Galilean satellites used in the thermal evolution calculation.

#### 4. Callisto

I model Callisto as a partially differentiated satellite with an inner core of water ice and silicate. This ice–silicate mixture region extends for 2213 km and the ice shell is 190 km thick (see Prentice, 2001 for details). The viscosity within the water ice–silicate core is given by

$$\eta(T_i) = \eta_0 \eta_r(\phi) \exp \left[ I \left( \frac{T_m(p)}{T} - 1 \right) \right], \quad (16)$$

where the relative viscosity,  $\eta_r$ , in Eq. (16) is a function of the silicate volume fraction,  $\phi = X_{\text{sil}}(\rho_{\text{core}}/\rho_{\text{sil}})$ , where  $\rho_{\text{core}}$  is the core mean density and  $X_{\text{sil}}$  is the mass fraction of silicate in the core (Friedson and Stevenson, 1983; Mangold et al., 2002),

$$\eta_r(\phi) = 1 + 2.5\phi + 10.05\phi^2 + 0.00273 \exp(16.6\phi). \quad (17)$$

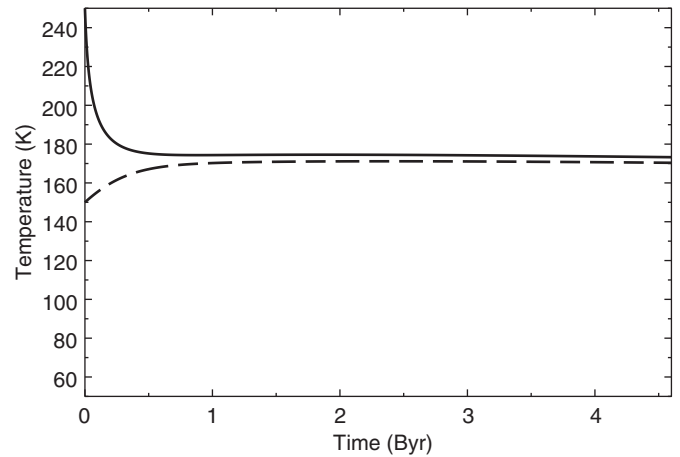


Fig. 4. Hot start versus cold start thermal evolution models. In both cases, the satellite is modeled as a two-layer satellite consisting of a silicate interior 60% of the satellite radius and an icy mantle 40% of the satellite radius (satellite radius is 2500 km). Other satellite parameters are given in Table 1. The heat flux between layers is calculated according to Eq. (12). For the hot start model (solid curve) the initial temperatures were  $T_{\text{silicate}} = 1800 \text{ K}$ ,  $T_{\text{ice}} = 250 \text{ K}$  and for the cold start model (dashed curve) the initial temperatures were  $T_{\text{silicate}} = 1500 \text{ K}$ ,  $T_{\text{ice}} = 150 \text{ K}$ . Both models result in comparable ice mantle temperatures for model times  $> 1 \text{ Byr}$ .

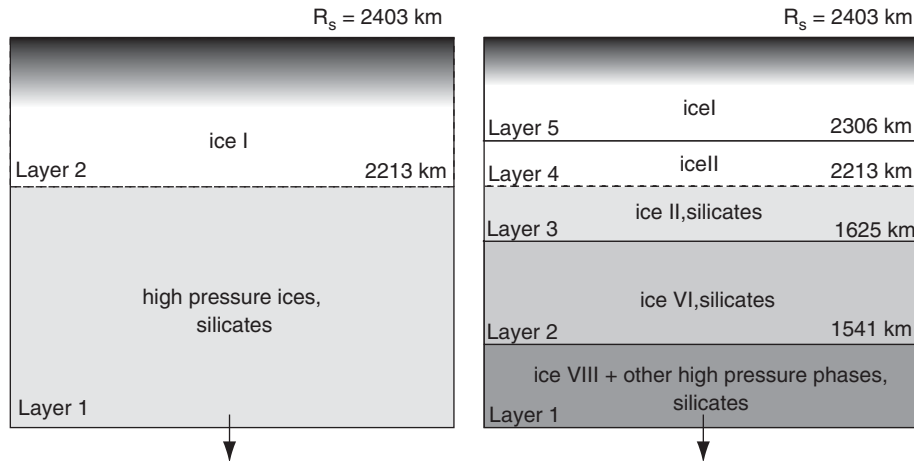


Fig. 5. Internal structure for Callisto used in the thermal evolution models.

The parameters used in the Callisto models are given in Table 1 and the satellite structure is shown in Fig. 5. I set the initial temperature in the water ice–silicate mixture interior to be  $T_{0,\text{mix}} = 105$  K and the initial temperature of the clean ice shell to be  $T_{0,\text{ice}} = 104$  K. For each model, I vary the zero-pressure melt viscosity of the water ice from  $10^{11}$ – $10^{14}$  Pa s.

#### 4.1. Callisto two-layer model

The calculated thermal and heat flux evolution of the satellite for  $\eta_0 = 10^{12}$  Pa s is given in Fig. 6. For all models, the viscosity of the hydrated silicate–water ice interior is controlled by the rheological parameters of water ice. All models indicate that the interior remains relatively cool for the entire evolution of the satellite with the temperature difference between the ice–silicate mixture core and the water ice mantle being at most  $\sim 50$  K for the model that used the Newtonian stagnant lid scaling law of Moresi and Solomatov (1995), Eq. (12), and as small as  $\sim 10$  K with the non-Newtonian  $n = 4$  scaling law of Eq. (14).

The heat flux evolution shown in Fig. 6 exhibits similar results for the present day surface heat flux for these models. The maximum satellite heat flux, however, occurs at different times for each model with the Newtonian stagnant lid scaling delaying the maximum heat flux for the satellite until about 2.5 Byr as opposed to earlier in the evolution of the satellite for the other scaling laws.

The isoviscous scaling law resulted in much cooler temperatures for both the core and mantle. Since the boundary layer thickness is small, heat is easily transported through the satellite by convection and the satellite remains cold. The non-Newtonian heat flux scaling laws both resulted in similar present day mantle temperatures, differing by 10 K. The non-Newtonian  $n = 3$  scaling law resulted in much larger core temperatures than the  $n = 4$  scaling law.

Similar present-day mantle temperatures and surface heat fluxes are seen for all models, yet the stagnant lid

scaling laws consistently result in warmer mantle internal temperatures than the isoviscous scaling law. In all cases the Newtonian stagnant lid law gave warmer mantle temperatures and larger present day surface heat fluxes. The non-Newtonian laws gave slightly cooler internal mantle temperatures than the Newtonian stagnant lid law with the  $n = 4$  rheology consistently resulting in colder present day mantle temperatures and lower surface heat fluxes.

The two-layer models for Callisto have all resulted in a cold satellite. Thermal convection within each layer was of sufficient vigor to efficiently remove the heat generated within the silicate rich portion of the satellite. The initial, nearly homogeneous structure of the satellite remains preserved to the present day. Melting of the water ice constituents is unlikely. However, the presence of add mixtures of volatile assemblages, such as ammonia ice, within the satellite interior will effect both the thermal evolution of the satellite and the present day structure (Kargel, 1992). Models with  $\eta_0 \geq 10^{12}$  Pa s all resulted in internal mantle and core temperatures that are in excess of the ammonia dihydrate solidus temperature of 176 K (Kargel, 1992).

#### 4.2. Callisto five-layer model

The structure of the satellite used in this model is shown in Fig. 3. In this model, Callisto is comprised of an inner high-density region of hydrated silicates and high-pressure ice phases over the region of radius 1541 km. Above this region the satellite has two further layers of hydrated silicates and water ice VI and II with the boundaries between the layers present at 1625 and 2213 km. The final two layers of the satellite are composed of water ice II and I with the boundary between the layers at 2306 km. The ice I layer extends to the surface of the satellite (Prentice, 2001).

The rheological properties of the dense ice phases of water ice are still subject to large uncertainties. Data describing the deformation style of ice phases larger than

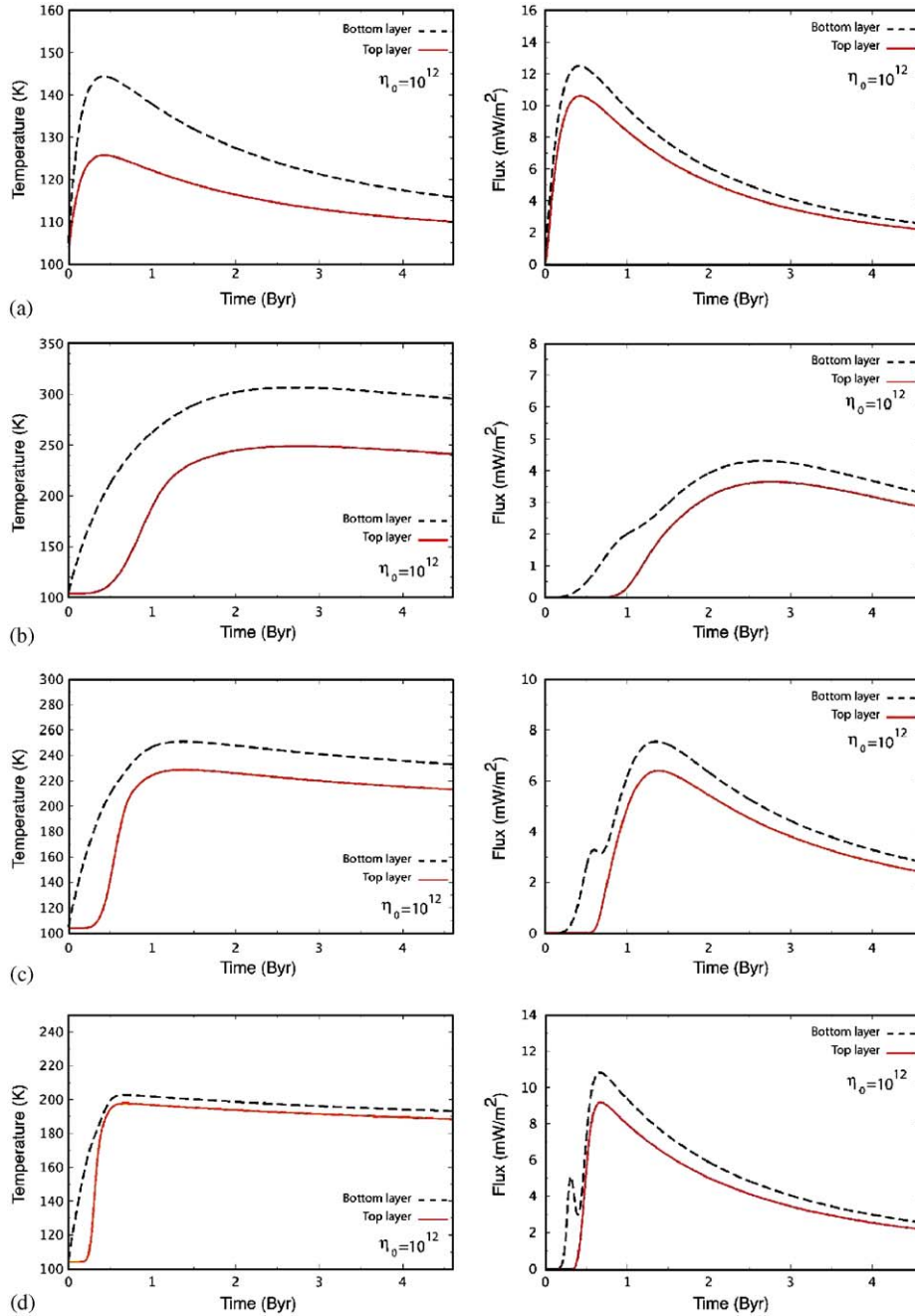


Fig. 6. Two-layer thermal and heat flux evolution of Callisto for  $\eta_{0,ice} = 10^{12}$  and  $\eta_{0,sil} = 10^{19}$ . (a) employs the isoviscous scaling law of Eq. (11), (b) Newtonian stagnant lid scaling law, Eq. (12), (c) non-Newtonian  $n = 3$  scaling law, Eq. (13) and (d) non-Newtonian  $n = 4$  scaling law, Eq. (14).

ice VI is scarce and in this study I assume that the deformation of the more dense phases follows the rheology of water ice VI. For water ices I, II and VI the rheological data given in Durham and Stern (2001) is employed, and the viscosity parameters for the higher ice phases is given in Table 1. The initial temperature in each layer was  $T_{0,1} = 150$  K,  $T_{0,2} = 140$  K,  $T_{0,3} = 130$  K,  $T_{0,4} = 120$  K,  $T_{0,5} = 110$  K and  $T_s = 103$  K (where subscripts refer to time, layer)—see Fig. 3).

The evolution of this five-layer Callisto model is shown in Fig. 7 for  $\eta_{0,ice} = 10^{12}$  Pa s. In this figure, the thermal

evolution of each layer in shown along with the corresponding heat flux that is exiting in that layer. Each graph in Fig. 7 corresponds to the thermal evolution of the satellite determined with the different heat flux scaling laws of Eqs. (11)–(14). For this set of model parameters, the isoviscous heat flux scaling law resulted in a cool Callisto model after an initial period of  $\sim 1$  Byr in which time the satellite heated up rapidly. The subsequent evolution of the satellite saw each layer cooling until a present day ice I mantle temperature of 206.53 K and a surface heat flux of  $5.263 \text{ mW m}^{-2}$  are attained.

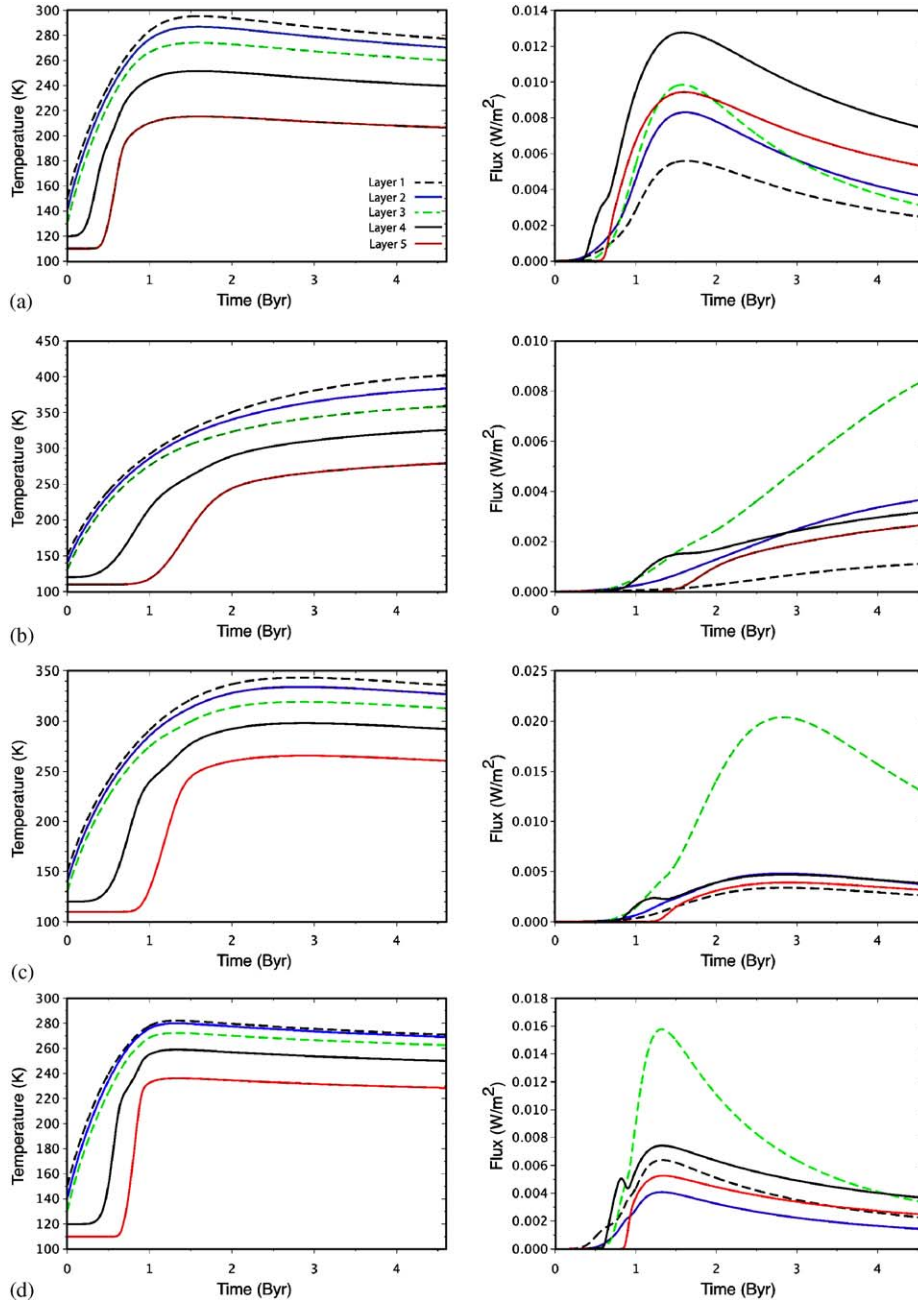


Fig. 7. Thermal and heat flux evolution for the five-layer Callisto model. Results shown are for  $\eta_{0,\text{ice}} = 10^{12}$  Pa s. Heat flux scaling law: (a) Eq. (11), (b) Eq. (12), (c) Eq. (13) and (d) Eq. (14).

The Callisto model calculated with the Newtonian stagnant lid scaling law, Eq. (12), is shown in Fig. 7b. Maximum values for the heat flows and layer temperatures were achieved at the end of the simulation. Inspection of the heat flux curves for each layer show a monotonically increasing curve for layer 3. This layer is the transition layer from water ice II and hydrated silicate species to the water ice II layer and the rate at which thermal energy is advected into this region will influence the thermal structure of the upper ice layers. The use of Eq. (12) has resulted in a very warm satellite interior. Internal temperatures are potentially greater than the pressure

dependent water ice melting temperature. Should these temperatures have been reached within the silicate-rich portion of the satellite then further differentiation of the satellite would ensue. Since the Galileo data suggests that Callisto is only partially differentiated, this thermal evolution scenario is not favored.

The bottom two graphs in Fig. 7 show the thermal evolution of the five-layer Callisto model when a non-Newtonian stagnant lid heat flux scaling laws are used in the thermal evolution calculation. These graphs define the evolution of Callisto when Eq. (13) (Fig. 7c) and Eq. (14) (Fig. 7d) are used. The  $n = 3$  law resulted in a cooling

satellite model after 2.5 Byr. The present day ice I mantle temperature is determined to be 260.62 K corresponding with a surface heat flux of  $3.15 \text{ mW m}^{-2}$ . The non-Newtonian  $n = 4$  scaling law results in rapid heating of the satellite interior early in the thermal evolution with the majority of the evolution spent cooling. The present day ice I layer temperatures for this model is 228.65 K and the present day surface heat flux is  $2.46 \text{ mW m}^{-2}$ .

The Newtonian stagnant lid viscosity scaling law resulted in hotter internal ice I layer temperatures and smaller surface heat fluxes than the non-Newtonian scaling laws over the range of viscosity parameters. This is in contrast to the results obtained for the non-Newtonian scaling laws. These show that the non-Newtonian stagnant lid  $n = 4$  law gave present day ice I layer temperatures that are  $\sim 30 \text{ K}$  cooler than the  $n = 3$  results, and  $\sim 20 \text{ K}$  cooler for maximum ice I layer temperatures. The  $n = 4$  scaling law resulted in a smaller surface heat flux than the  $n = 3$  law for all variations in the viscosity prefactor value.

### 5. Ganymede

The internal structure of Ganymede is shown in Figs. 3 and 8. I present the results of the thermal evolution calculation for two structural models of Ganymede. The first model is a simple two zone structure comprised of a dehydrated silicate core of radius 1663 km overlain by a water ice mantle 971 km thick. The rheological properties of the whole water ice mantle are assumed to follow that of water ice I. The structure of the two zone model is shown in Fig. 7. The initial temperatures in each layer is chosen to be  $T_{0,1} = 900 \text{ K}$  and  $T_{0,2} = 200 \text{ K}$ .

A five-layer satellite model has also been constructed. Assuming hydrostatic equilibrium throughout the satellite, the high-density water ice phase boundaries are assumed to be present at the following radii: ice VIII  $\rightarrow$  ice VI at 1725 km, ice VI  $\rightarrow$  ice II at 1815 km and ice II  $\rightarrow$  ice I at 2577 km. Within the satellite, heat production due to the decay of radioactive isotopes is occurring only in the silicate core. The initial

temperatures in each layer is  $T_{0,1} = 600 \text{ K}$ ,  $T_{0,2} = 250 \text{ K}$ ,  $T_{0,3} = 220$ ,  $T_{0,4} = 200 \text{ K}$ ,  $T_{0,5} = 170 \text{ K}$  and  $T_s = 103 \text{ K}$ . Material parameters for each layer are given in Table 1.

#### 5.1. Ganymede two-layer model

The results for the two-zone Ganymede thermal model for  $\eta_{0,\text{ice}} = 10^{12} \text{ Pa s}$  and two values of  $\eta_{0,\text{sil}} = 10^{19} \text{ Pa s}$  and  $10^{21} \text{ Pa s}$ , and the heat flux scaling laws given in Eqs. (11)–(14) are shown in Fig. 9.

The isoviscous heat flux scaling relationship of Eq. (11) has resulted in a thermal evolution that is characterized by a hot silicate interior and a relatively uniform water ice mantle temperature. The more viscous silicate model with  $\eta_{0,\text{sil}} = 10^{21} \text{ Pa s}$ , gives silicate core temperatures that are  $\sim 100 \text{ K}$  greater than those of the  $\eta_{0,\text{sil}} = 10^{19} \text{ Pa s}$  model. This difference in the evolution of the silicate region of the satellite is also reflected in the temporal evolution of the heat flux within each distinct rheological zone. The low viscosity silicate model heat fluxes that peak early, whilst the more viscous model delayed the maximum heat flux until a later time.

Solving the energy balance equations with a Newtonian stagnant lid heat flux scaling relationship resulted in a hotter silicate core and a corresponding reduction in the heat flux exiting each layer when compared to the isoviscous model. The Newtonian stagnant lid scaling law results in significantly warmer interior layer temperatures than those achieved using the isoviscous heat flux scaling law. This is in agreement with the results of numerical simulations (Moresi and Solomatov, 1995). Silicate layer temperatures in this model are very large, suggesting that dehydration of the silicate interior is likely and that the separation between silicate materials and metals is also possible.

The build up of heat beneath the stagnant lid of the model results in lower heat fluxes over the evolution of the satellite. The present day mantle temperature for these models are found to be:  $277.58 \text{ K}$  for the model with  $\eta_{0,\text{sil}} = 10^{19} \text{ Pa s}$  and  $\eta_{0,\text{ice}} = 10^{12} \text{ Pa s}$  and  $251.30 \text{ K}$  for the  $\eta_{0,\text{sil}} =$

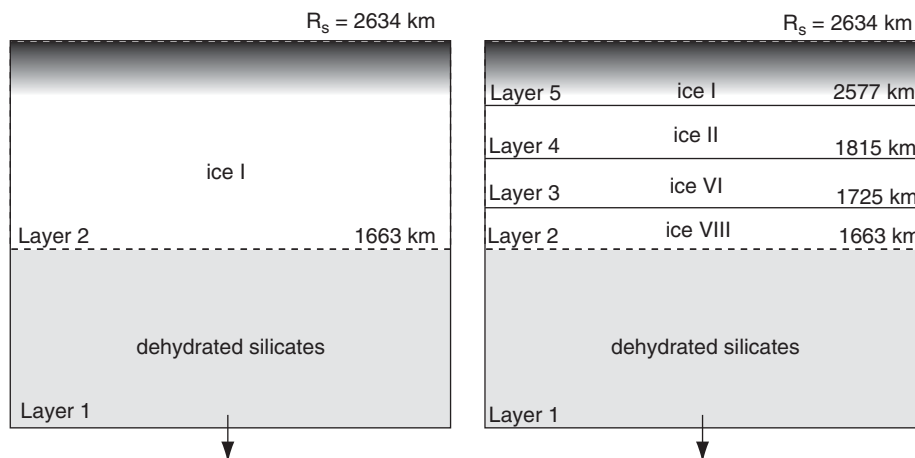


Fig. 8. Internal structure for Ganymede used in the thermal evolution models.

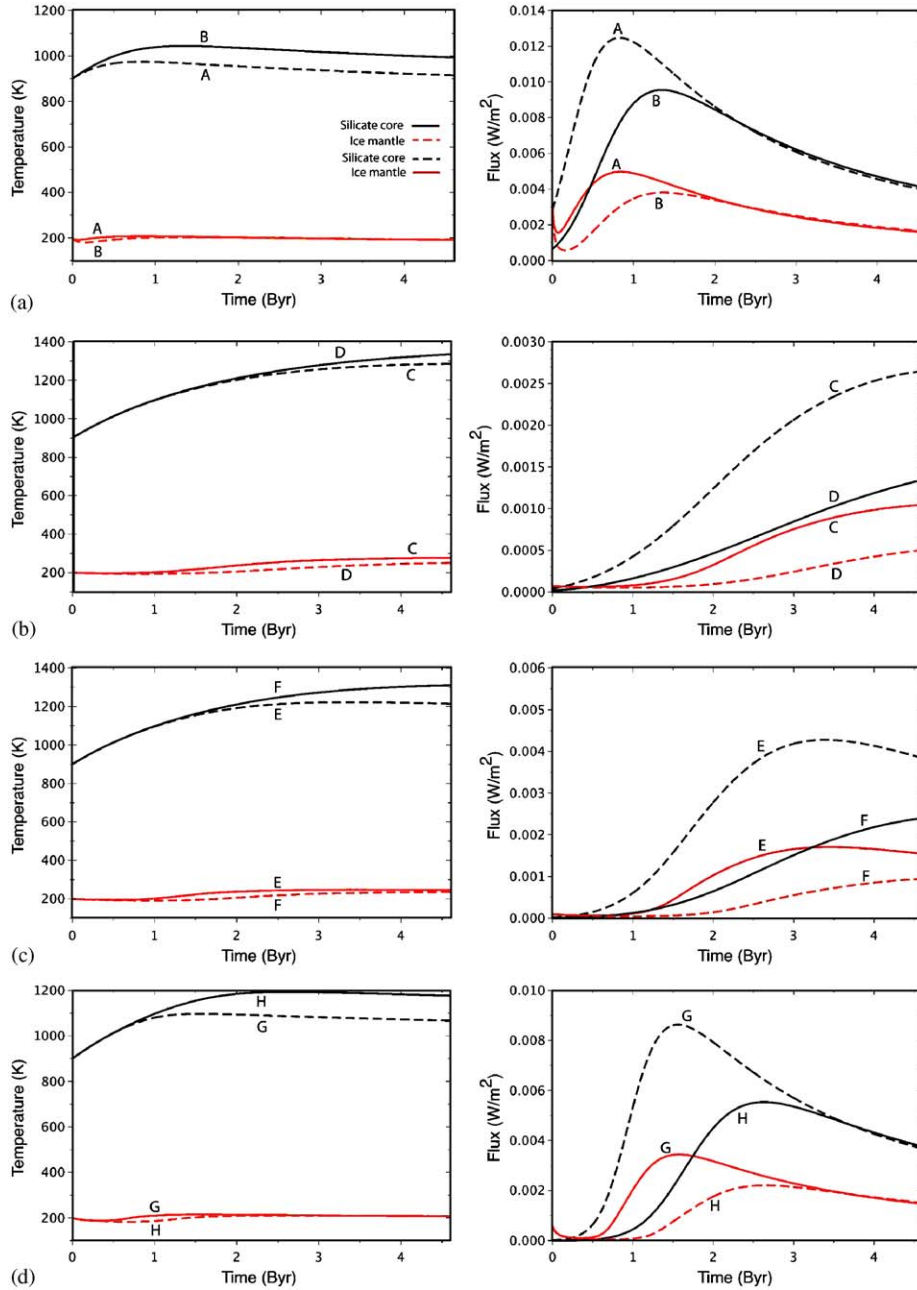


Fig. 9. Two-layer Ganymede thermal evolution results. for  $\eta_{0,\text{ice}} = 10^{12}$  Pa s and  $\eta_{0,\text{sil}} = 10^{19}, 10^{21}$  Pa s. Models A, C, E and G use  $\eta_{0,\text{ice}} = 10^{12}$  Pa s and  $\eta_{0,\text{sil}} = 10^{19}$  Pa s, models B, D, F and H use  $\eta_{0,\text{ice}} = 10^{12}$  Pa s and  $\eta_{0,\text{sil}} = 10^{21}$  Pa s. Models A and B employ the heat flux scaling law of 11, models C and D use Eq. (12), models E and F use Eq. (13) and models G and H use Eq. (14).

$10^{21}$  Pa s and  $\eta_{0,\text{ice}} = 10^{12}$  Pa s model. With a mantle temperature  $> 277$  K, melting of the ice is likely since the water ice solidus curve as a function of pressure reaches a minimum at  $\sim 255$  K at 0.21 GPa (Hobbs, 1974).

The  $n = 3$  non-Newtonian viscosity scaling law results in hot silicate interiors for models having both of the silicate viscosity pre-factor value. As for the isoviscous case, the lower viscosity model is  $\sim 100$  K cooler than the high viscosity model. Water ice mantle temperatures remain uniform over the evolution time and both models gave similar present day mantle temperatures. The heat flux

evolution is very different from the Newtonian model for both the present day surface heat flux and the heat flux at the core mantle boundary, due to the presence of the stagnant lid. As with the Newtonian stagnant lid models, silicate interior temperatures are sufficiently high to allow for the separation between metals and rock and the formation of a metallic core and presence of a magnetic field at Ganymede is suggestive of such an inner metallic core (Schubert et al., 1996).

The final evolution calculation for the two layer Ganymede model employed the  $n = 4$  scaling law (Eq. (14)). This model

displays similar evolution features to the non-Newtonian stagnant lid  $n = 3$  result with comparable silicate core and water ice mantle temperatures. Again, the more viscous silicate interior model has resulted in internal silicate layer temperatures that are  $\sim 100$  K greater than the less viscous model. This model also shows that a maximum temperature is reached in the silicate interior early in the simulation at  $\sim 2$  Byr. This maximum temperature is reflected in the heat flux evolution curves for each model.

The isoviscous scaling law models give the coolest satellite interior temperatures and a larger surface heat flux when compared with the corresponding model for the other heat flux scaling relationships. Comparisons between the stagnant lid models for both the Newtonian and non-Newtonian scaling laws shows that the Newtonian stagnant lid scaling law results in the highest temperature interiors and the lowest surface heat fluxes for all viscosity models. In many cases the melting temperatures of materials within the satellite's interior are achieved, with the high viscosity models achieving temperatures greater than the water ice solidus temperature.

## 5.2. Ganymede five-layer model

The thermal evolution of the five-layer Ganymede model is given in Fig. 10 for values of the parameters  $\eta_{0,\text{sil}} = 10^{19}$  Pa s and  $\eta_{0,\text{ice}} = 10^{12}$  Pa s and for each of the heat flux scaling laws in Eqs. (11)–(14).

The Newtonian isoviscous heat flux scaling law for the viscosity parameters specified above gives a thermal evolution model for Ganymede that results in a hot silicate core with a present day temperature of  $\sim 910$  K and an ice I layer temperature  $\sim 182$  K. The present day surface heat flux for this model is  $\sim 0.8$  mW m $^{-2}$ . The water ice layers show little change from their initial starting temperatures with a slight increase in layer temperature after 2.5 Byr. Heat transfer through each layer shows an increase in the heat flux after this time. This is because the silicate interior has become convective. The differing rheologies of the layers, coupled with an isoviscous heat transfer scaling relationship, has little effect on the evolution of the satellite with this model displaying similar characteristics to the previously described two-layer isoviscous model.

Solving the heat transfer problem with a Newtonian stagnant lid heat flux scaling law has resulted in a decrease in the heat flux transferred between layers. In this model, the extensive silicate core retains most of its thermal energy trapped beneath a large thermal boundary layer. Comparison of the silicate interior temperatures with the isoviscous model shows that the Newtonian stagnant lid scaling law results in core temperatures  $\sim 100$  K warmer. Subsequently, there is little thermal energy to drive the evolution of the water ice layers. The high-pressure ice VIII layer does show a modest increase in temperature over the simulation time, but this increase is insufficient to lead to any significant thermal evolution of the outer water ice layers. In fact, the

outer water I layer steadily cools from its initial temperature of 170 K to a present day value of 147.58 K.

The non-Newtonian,  $n = 3$  stagnant lid scaling law exhibits a very similar evolution to that of the Newtonian stagnant lid scaling law. Silicate core temperatures increase over simulation time to a present day value of  $\sim 950$  K and the overlying water ice layers display little temperature evolution. As for the Newtonian stagnant lid scaling law model, heat transfer between layers is negligible and the present day surface heat flux is three orders of magnitude smaller than the isoviscous scaling law model. Again, the outer ice I layer cools to a present day value of 162.48 K from an initial temperature of 170 K.

The non-Newtonian,  $n = 4$  heat flux scaling law results in a present day silicate interior temperature of  $\sim 1000$  K. As in the previous models, the ice layers show little temperature evolution with a small increase in inner layer temperatures after 3.5 Byr. It is also at this time that the heat flux between layers begins to increase. The present day surface heat flux from the cold water ice I layer is three orders of magnitude smaller than the isoviscous model.

## 6. Discussion

Parameterized thermal convection models for the large icy satellites Ganymede and Callisto were calculated using an isoviscous, Newtonian stagnant lid, and two non-Newtonian stagnant lid heat flux scaling laws. Numerical investigations of stagnant lid convection in 2D cartesian and 3D spherical geometry have shown that thermal convection within the stagnant lid regime results in warmer internal temperatures than isoviscous thermal convection. Further, the heat flux scaling laws for stagnant lid convection are significantly different from the Rayleigh number–Nusselt number scaling laws obtained from theoretical, numerical and laboratory studies of isoviscous thermal convection. This study has shown that the heat flux scaling law employed by a parameterized convection study strongly influences the thermal evolution of the body.

The calculated thermal evolution of Callisto shows this body to have a cool, convective interior. Application of the four heat flux scaling laws resulted in present day conditions for Callisto that differ by at most 50 K for mantle temperatures and 0.719 mW m $^{-2}$  for the surface heat flux. The isoviscous scaling law resulted in cold Callisto models whilst the stagnant lid scaling laws resulted in warmer internal temperatures for the satellite. In some instances (e.g.  $\eta_{0,\text{ice}} > 10^{11}$  Pa s), melting of the water ice component of the satellite was achieved. Additional volatile ices incorporated into the bulk chemical composition of the satellite, such as ammonia, will reduce the melting temperature even further. Ammonia dihydrate has a 0 GPa pressure melting temperature of 176 K (Kargel, 1992). All models with  $\eta_{0,\text{ice}} > 10^{11}$  Pa s achieved internal water ice I layer temperatures larger than this value. The detection of an induced magnetic field signature about Callisto by the Galileo spacecraft magnetometer (Kivelson

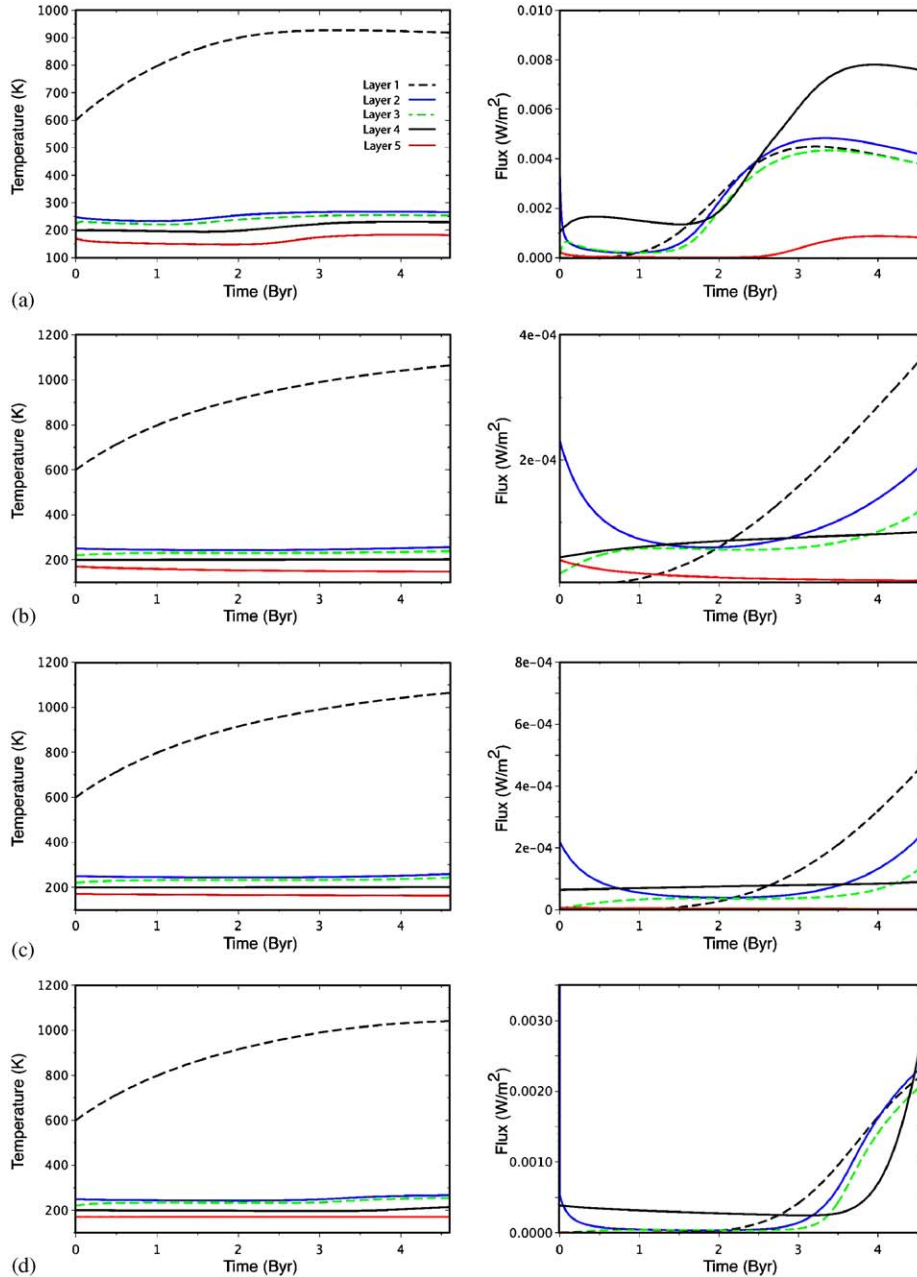


Fig. 10. Five-layer Ganymede model results for  $\eta_{0,\text{ice}} = 10^{12}$  Pa s and  $\eta_{0,\text{sil}} = 10^{19}$  Pa s. Heat flux scaling law is: (a) Eq. (11), (b) Eq. (12), (c) Eq. (13) and (d) Eq. (14).

et al., 1999; Zimmer et al., 2000) is explained by the presence of a salty subsurface ocean (Prentice and Freeman, 1999) or a subsurface liquid water ocean (Ruiz, 2001). The stagnant lid satellite models presented for Callisto provide one mechanism through which internal temperatures may easily reach the melt temperature of the constituent icy materials.

Two- and five-layer models for Ganymede with an isoviscous scaling law resulted in cooler internal temperatures than those of the non-Newtonian scaling law models. The Newtonian stagnant lid scaling law resulted in the warmest Ganymede models whilst the non-Newtonian  $n = 4$  scaling law gave intermediate thermal evolution models.

Ganymede models with high silicate and water ice viscosities gave internal temperatures which were above the water ice melting temperature. The presence of an internal ocean on Ganymede has been suggested (Moore and Schubert, 2003). Inversion of the Galileo magnetic field data for Ganymede, unlike Callisto, is complicated by the fact that Ganymede possesses a native magnetic field, generated either by thermoremanent magnetization of  $\text{Fe}_3\text{O}_4$  contained in a metal-silicate core (Crary and Bagenal, 1998), or generated through the presence of a central metallic (Fe or FeS) core (Gurnett et al., 1996; Schubert et al., 1996; Kivelson et al., 1996). Silicate core temperatures for both the two-layer and five-layer

Ganymede models show that with a stagnant lid scaling law the internal temperature of the silicate core is high enough to facilitate the further differentiation of silicate and metal species. Structural models by Anderson et al. (1996) suggest that an internal metallic core within Ganymede may be up to 50% of the satellites radius.

This highlights the effect of one of the important parameters controlling the thermal evolution of the large icy Galilean satellites—namely, the viscosity of the water ice. It should be cautioned that the viscosity of water ice in the planetary environment is not well constrained and the extrapolation of terrestrial water ice data to planetary conditions is subject to large uncertainties. Strain rates within a large icy satellite like Ganymede or Callisto are expected to be of the order  $\dot{\epsilon} \sim 10^{-14} \text{ s}^{-1}$ , whilst most laboratory experiments are performed in the range  $10^{-7} < \dot{\epsilon} < 10^{-4} \text{ s}^{-1}$  (Durham and Stern, 2001). In this sense, the laboratory data is an upper bound on the rheological properties of water ice. Deschamps and Sotin (2001) used the results of the Gerrard et al. (1952) alpine glacier study to infer that the reference viscosity in Eq. (5) is  $5 \times 10^{13} \text{ Pa s}$  for a strain rate of  $\dot{\epsilon} \sim 10^{-11} \text{ s}^{-1}$ . This value is inline with the large viscosity models of this study, and many of the stagnant lid models having  $\eta_{0,\text{ice}} > 10^{13}$  resulted in mantle temperatures greater than the water ice melt temperature. With this value for  $\eta_{0,\text{ice}}$  subsurface liquid oceans may exist inside many of the large icy moons of the solar system.

In this study I have assumed that the internal heating rate of each satellite was derived from radiogenic decay within the silicate mass fraction. Residual accretional heat and external heat sources, such as that derived from friction due to tidal flexing of the satellite as it orbits around Jupiter have not been included. The addition of these heat sources will act to increase the possibility of melting a water ice mantle (this effect is thought to be more important for Europa than Ganymede or Callisto, although Ganymede may have been subjected to some tidal heating at some time in its history (Showman et al., 1997)).

Studies of thermally driven convection in the mantle of the Earth suggest that phase transitions have a significant influence on the thermal history of the planet (Tackley, 1995). Christensen and Yuen (1984, 1985) found that the important driver for mantle convection where a phase transition exists is the density change upon going through a phase transition. The influence of phase boundaries on icy satellite convection has been discussed by Thurber et al. (1980), Bercovici et al. (1986) and Sotin and Parmentier (1989). Layered convection models result in warmer internal temperatures (McKinnon, 1998), a result that is confirmed by this study. Further numerical investigations into icy mantle convection with phase transitions are required to fully explore the implications that water ice phase transitions have on the thermal evolution of the body.

The current suite of thermal evolution models represent only a narrow slice through the parameter space. Many of the controlling parameters are subject to large uncertainty. The parameters chosen in this study are those thought to

have the most influence to the thermal evolution of the satellite. The main purpose of this study has been to explore the influence which various scaling laws, defined in Eqs. (11)–(14), have on the thermal evolution.

## 7. Conclusion

It has been shown that isoviscous Rayleigh number–Nusselt number scaling laws result in cooler thermal evolution models for the large icy Galilean satellites when compared to the results for Newtonian and non-Newtonian stagnant lid scaling laws. With a stagnant lid heat flux scaling law, internal water ice mantle temperatures may exceed than the water ice solidus temperature, resulting in extensive melting of the mantle and the formation of subsurface oceans. The thermal evolution models for Callisto suggest that this satellite has remained cool over its evolution to present day, whilst Ganymede has evolved to be a much warmer body. All of the icy Galilean satellites may possess subsurface oceans, and stagnant lid thermal convection is one mechanism through which such an ocean may form.

## Acknowledgment

I wish to thank the editor, Nadir Noor and an anonymous reviewer whose comments greatly improved the clarity of the paper. I also thank A.J.R. Prentice for helpful comments.

## References

- Anderson, J.D., Lau, E.L., Sjogren, W.L., Scubert, G., Moore, W.B., 1996. Gravitational constraints on the internal structure of Ganymede. *Nature* 384, 541–543.
- Anderson, J.D., Lau, E.L., Sjogren, W.L., Scubert, G., Moore, W.B., 1997. Gravitational evidence for an undifferentiated Callisto. *Nature* 387, 264–266.
- Anderson, J.D., Scubert, G., Jacobson, R.A., Lau, E.L., Moore, W.B., Sjogren, W.L., 1998a. Distribution of rock, metals and ices in Callisto. *Science* 280, 1573–1576.
- Bercovici, D., Schubert, G., Reynolds, R.T., 1986. Phase transitions and convection in icy satellites. *Geo. Res. Lett.* 13 (5), 448–451.
- Christensen, U.R., Yuen, D.A., 1984. The interaction of a subducting lithospheric slab with a chemical or phase boundary. *J. Geophys. Res.* 89, 4389–4402.
- Christensen, U.R., Yuen, D.A., 1985. Layered convection induced by phase transitions. *J. Geophys. Res.* 90, 10,291–10,300.
- Crary, F.J., Bagenal, F., 1998. Remanent ferromagnetism and the interior structure of Ganymede. *J. Geophys. Res.* 103 (E11), 25,757–25,773.
- Davaille, A., Jaupart, C., 1993. Transient high Rayleigh number thermal convection with large viscosity variations. *J. Fluid Mech.* 253, 141–166.
- Deschamps, F., Sotin, C., 2001. Thermal convection in the outer shell of large icy satellites. *J. Geophys. Res.* 106 (5), 107–121.
- Dombard, A.J., McKinnon, W.B., 2000. Long-term retention of impact crater topography on Ganymede. *Geophys. Res. Lett.* 27 (22), 3663–3666.
- Dombard, A.J., McKinnon, W.B., 2001. Formation of grooved terrain on Ganymede: extensional instability mediated by cold, superplastic creep. *Icarus* 154, 321–336.
- Durham, W.B., Stern, L.A., 2001. Rheological properties of water ice—applications to satellites of the outer planets. *Annu. Rev. Earth Planet. Sci.* 29, 295–330.

- Durham, W.B., Kirby, S.H., Stern, L.A., 1992. Effects of dispersed particulates on the rheology of water ice at planetary conditions. *J. Geophys. Res.* 97 (20), 883–897.
- Ellsworth, K., Schubert, G., 1983. Saturn's icy satellites: thermal and structural models. *Icarus* 54, 490–510.
- Freeman, J., Moresi, L., May, D., 2004. Evolution into the stagnant lid regime with a non-Newtonian water ice rheology. *Geophys. Res. Lett.* 31 (L11701), doi: 10.1029/2004GL019798.
- Friedson, A.J., Stevenson, D.J., 1983. Viscosity of rock-ice mixtures and applications to the evolution of icy satellites. *Icarus* 56, 1–14.
- Fowler, A.C., 1985. Fast thermoviscous convection. *Stud. Appl. Math.* 72, 189–219.
- Gerrard, J.A.F., Perutz, M.F., Roch, A., 1952. Measurement of the velocity distribution along a verticle line through a glacier. *Proc. R. Soc. London A* 207, 554–572.
- Goldsby, D.L., Kohlstedt, D.L., 2001. Superplastic deformation of ice: experimental observations. *J. Geophys. Res.* 106, 11,017–11,030.
- Greeley, R., Klemaszewski, J.E., Wagner, R., the Galileo Imaging Team, 2000. Galileo views of the geology of Callisto. *Planet. Space Sci.* 48, 829–853.
- Gurnett, D.A., et al., 1996. Evidence for a magnetosphere at Ganymede from plasma wave observations by the Galileo spacecraft. *Nature* 384, 535–537.
- Gurnett, D.A., Kurth, W.S., Roux, A., Bolton, S.J., 1997. Absence of a magnetic-field signature in plasma-wave observations at Callisto. *Nature* 387, 261–262.
- Hansen, U., Yuen, D.A., 1993. High Rayleigh number regime of temperature-dependent viscosity convection and the Earth's early thermal history. *Geophys. Res. Lett.* 20, 2191–2194.
- Hobbs, P.V., 1974. *Ice Physics*. Oxford University Press, London.
- Honda, S., 1995. A simple parameterized model of Earth's thermal history with the transition from layered to whole mantle convection. *Earth Planet. Sci. Lett.* 131, 357–369.
- Honda, S., Iwase, Y., 1996. Comparison of the dynamic and parameterized models of mantle convection including core cooling. *Earth Planet. Sci. Lett.* 139, 131–145.
- Hussmann, H., Spohn, T., Wiczerkowski, K., 2002. Thermal equilibrium states of Europa's ice shell: implications for internal ocean thickness and surface heat flow. *Icarus* 156, 143–151.
- Karato, S., Wu, P., 1993. Rheology of the upper mantle—a synthesis. *Science* 260, 771–778.
- Kargel, J.S., 1992. Ammonia–water volcanism on icy satellites: phase relations at 1 atmosphere. *Icarus* 100, 556–574.
- Khurana, K.K., Kivelson, M.G., Russel, C.T., Walker, R.J., Southwood, D.J., 1997. Absence of an internal magnetic field at Callisto. *Nature* 387, 262–264.
- Kirk, R.L., Stevenson, D.J., 1987. Thermal evolution of a differentiated Ganymede and implications for surface features. *Icarus* 69, 91–134.
- Kivelson, M.G., et al., 1996. Discovery of Ganymede's magnetic field by the Galileo spacecraft. *Nature* 384, 537–541.
- Kivelson, M.G., Khurana, K.K., Stevenson, D.J., Bennett, L., Joy, S., Russell, C.T., Walker, R.J., Zimmer, C., Polanskey, C., 1999. Europa and Callisto: induced or intrinsic fields in a periodically varying plasma environment. *J. Geophys. Res.* 104, 4609–4625.
- Mangold, N., Allemand, P., Duval, P., Geraud, Y., Thomas, P., 2002. Experimental and theoretical deformation of ice–rock mixtures: implications on rheology and ice content of Martian permafrost. *Planet. Space Sci.* 50, 385–401.
- McKinnon, W.B., 1997. Mystery of Callisto: is it undifferentiated?. *Icarus* 130, 540–543.
- McKinnon, W.B., 1998. Geodynamics of icy satellites. In: Schmitt, B., et al. (Eds.), *Solar System Ices*. Kluwer Academic Publishers, Dordrecht, pp. 525–550.
- McKinnon, W.B., Parmentier, E.M., 1986. Ganymede and Callisto Satellites. In: Burns, J.A., Shapley, M. (Eds.). *The University of Arizona Press, Arizona*, pp. 718–763.
- McNamara, A.K., van Keken, P.E., 2000. Cooling of the Earth: a parameterized convection study of whole versus layered models, *G Cubed* 1.
- Moore, W.B., Schubert, G., 2003. The tidal response of Ganymede and Callisto with and without liquid water oceans, *Icarus* 166, 223–226.
- Moresi, L.-N., Solomatov, V.S., 1995. Numerical investigation of 2D convection with extremely large viscosity variations. *Phys. Fluids* 7 (9), 2154–2162.
- Morris, S., Canright, D., 1984. A boundary layer analysis of Benard convection in a fluid of strongly temperature-dependent viscosity. *PEPI* 36, 355–373.
- Mueller, S., McKinnon, W.B., 1988. Three-layered models of Ganymede and Callisto: compositions, structures and aspects of evolution. *Icarus* 76, 437–464.
- Nataf, H.C., Richter, F.M., 1982. Convection experiments in fluids with highly temperature-dependent viscosity and the thermal evolution of the planets. *PEPI* 29, 320–329.
- Ogawa, M., Schubert, G., Zebib, A., 1991. Numerical simulations of three-dimensional thermal convection in a fluid with strongly temperature-dependent viscosity. *J. Fluid Mech.* 233, 299–328.
- Prentice, A.J.R., 2001. Origin, bulk chemical composition and physical structure of the Galilean satellites of Jupiter: a post-Galileo analysis. *Earth Moon Planets* 87, 11–55.
- Prentice, A.J.R., Freeman, J.C., 1999. Origin of Callisto and its subsurface electrolytic ocean. *Eos Trans. AGU* 80 (46), F607.
- Richter, F.M., Nataf, H.C., Daly, S.F., 1983. Heat transfer and horizontally averaged temperature of convection with large viscosity variations. *J. Fluid Mech.* 129, 173–192.
- Ruiz, J., 2001. The stability against freezing of an internal liquid–water ocean in Callisto. *Nature* 412, 409–411.
- Schenk, P.M., McKinnon, W.B., Gwynn, D., Moore, J.M., 2001. Flooding of Ganymede's bright terrains by low-viscosity water–ice lavas. *Nature* 410, 57–60.
- Schubert, G., Cassen, P., Young, R.E., 1979. Subsolidus convective cooling histories of terrestrial planets. *Icarus* 38, 192–211.
- Schubert, G., Stevenson, D.J., Ellsworth, K., 1981. Internal structures of the Galilean satellites. *Icarus* 47, 46–59.
- Schubert, G., et al., 1996. The magnetic field and internal structure of Ganymede. *Nature* 384, 544–545.
- Showman, A.P., Stevenson, D.J., Malhotra, R., 1997. Coupled orbital and thermal evolution of Ganymede. *Icarus* 129, 367–383.
- Solomatov, V.S., 1995. Scaling of temperature- and stress-dependent viscosity convection. *Phys. Fluids* 7 (2), 266–274.
- Solomatov, V.S., Moresi, L.N., 1997. Three regimes of mantle convection with non-Newtonian viscosity and stagnant lid convection on the terrestrial planets. *Geophys. Res. Lett.* 24, 1907–1910.
- Solomatov, V.S., Moresi, L.N., 2000. Scaling of time-dependent stagnant lid convection: application to small scale convection on Earth and other terrestrial planets. *J. Geophys. Res.* 105, 21,795–21,817.
- Sotin, C., Parmentier, E.M., 1989. On the stability of a fluid layer containing a univariant phase transition: application to planetary interiors. *Phys. Earth Planet. Inter.* 55, 10–25.
- Spohn, T., Schubert, G., 1982. Modes of mantle convection and the removal of heat from the Earth's interior. *J. Geophys. Res.* 87, 4682–4696.
- Stevenson, D.J., Spohn, T., Schubert, G., 1983. Magnetism and the thermal evolution of the terrestrial planets. *Icarus* 54, 466–489.
- Tackley, P.J., 1995. Mantle dynamics: influence of the transition zone. *Rev. Geophys. suppl.* 33, 275–282.
- Thurber, C.H., Hsui, A.T., Toksoz, M.N., 1980. Thermal evolution of Ganymede and Callisto: effects of solid state convection and constraints from Voyager imagery. In: *Proceedings of Lunar Planetary Science 11th Conference*, pp. 1957–1977.
- Turcotte, D.L., Schubert, G., 1982. *Geodynamics: Applications of Continuum Physics to Geological Problems*. Wiley, New York.
- Zhanle, K., Dones, L., Levison, H.F., 1998. Cratering rates on the Galilean satellites. *Icarus* 136, 202–222.
- Zimmer, C., Khurana, K.K., Kivelson, M.G., 2000. Subsurface oceans on Europa and Callisto: constraints from Galileo magnetometer observations. *Icarus* 147, 329–347.